Supramolecular Assembly of U(IV) Clusters and Superatoms

Ian Colliard,[1] Gregory Morrison,[2] Hans-Conrad zur Loye[2] and May Nyman[1*]

[1]Department of Chemistry, Oregon State University, Corvallis, OR 97331, USA
[2]Department of Chemistry and Biochemistry, University of South Carolina, Columbia, South Carolina 29208, USA

*correspondence: may.nyman@oregonstate.edu

Abstract: Superatoms are nanometer-sized molecules or particles that can form ordered lattices, mimicking their atomic counterparts. Hierarchical assembly of superatoms gives rise to emergent properties in superlattices of quantum-dots, p-block clusters, and fullerenes. Here, we introduce a family of uranium-oxysulfate cluster anions whose hierarchical assembly in water is controlled by two parameters; acidity and the countercation. In acid, larger Ln^{III} (Ln=La-Ho) link hexamer (U_6) oxoclusters into body-centered cubic frameworks, while smaller Ln^{III} (Ln=Er-Lu &Y) promote linking of fourteen U_6-clusters into hollow superclusters (U_{84} superatoms). U_{84} assembles into superlattices including cubic-closest packed, body-centered cubic, and interpenetrating networks, bridged by interstitial countercations, and U_6-clusters. Divalent transition metals (TM=Mn^{II} and Zn^{II}), with no added acid, charge-balance and promote the fusion of 10 U_6 and 10 U-monomers into a wheel–shaped cluster (U_{70}). Dissolution of U_{70} in organic media reveals (by small-angle X-ray scattering) that differing supramolecular assemblies are accessed, controlled by TM-linking of U_{70}-clusters.

Introduction:

Molecular fractals and supramolecular assemblies are studied to understand the underlying rules of complex assemblies and to access materials and molecules with multiscale properties. Molecular fractals are strategically synthesized via organic and coordination chemistry in metallocycles,[1, 2] dendrimers,[3, 4, 5] and proteins.[6] Inorganic materials that exhibit multiscale structure replication via supramolecular assembly are rare. Rather, these phenomena have been observed at a non-molecular level, in the self-assembly of nanomaterials including CdSe nanorods,[7] and silver nanosheets.[8] Bimodal, monodisperse nanoparticles with organic capping groups, C_{60}-fullerenes[9] behave as 'superatoms', assembling into lattices that resemble binary compound structure types.[10] In addition, semiconducting p-block Zintl-cluster anions[11] (i.e. As_7^{3-}, Al_{13}^{1-}) can be assembled through counteraction linking into different structures that exhibit structure specific electronic properties.[12, 13]

Several inorganic and metal-organic materials that represent revolutionary discoveries are built via supramolecular assembly of polynuclear metal-oxo clusters, including synthetic zeolites and metal-organic frameworks (MOFs). The UiO-66[14] MOF, widely exploited for its stability and adaptability to different applications, is built of hexanuclear, **Zr_6** oxo-clusters, isostructural with

U₆ (described later). A cluster building block of zeolites consists of eight corner-linked $(Al,Si)O_4$ tetrahedra, and these clusters have been both isolated in the molecular form[15, 16] and shown to self-assemble in solution[17] prior to crystallization of zeolites. In between isolated polynuclear cluster molecules and infinite lattices built from such clusters, is any number of hypothetical entities; i.e. assemblies of clusters, or pre-nucleation 'clusters of clusters'. As a rare example of these, metal organic polyhedra, MOPs, were designed and developed almost in parallel with MOFs, consisting of small cages joined by ditopic linkers.[18, 19] There is no analogous inorganic molecule that represents a scale between a cluster building-block and an infinite lattice, because inorganic synthesis generally does not allow for precise size control at such a large scale.

Assembly of actinide clusters into materials is likewise of interest but far less prolific. One of the most common cluster motifs is the aforementioned hexamer $[M^{IV}_6(OH)_4(O)_4)]^{12+}$ (M=An including Th, U, Np, Pu, also Zr/Hf) stabilized by various carboxylate groups, triflates, selenate, and sulfate.[20, 21, 22 23, 24] Researchers have synthesized MOFs and inorganic frameworks (including interpenetrating frameworks[23]) featuring linked **Th₆**,[23, 25, 26] **U₆**,[27, 28] and **Np₆**[29] nodes. The An_6 cluster is also an exact building block of AnO_2. Recently, clusters ranging in nuclearity from An_{10}-An_{38} have been isolated that are larger fragments of AnO_2,[30, 31, 32, 33, 34, 35, 36] elucidating understanding of colloidal actinide transport in the environment.[37] **U^{IV}**-sulfate speciation (with heterometals) is of special relevance to biogeochemical activity in uranium ore deposits, mining sites and the contaminated subsurface. Sulfur oxidizing bacteria immobilizes uranium as discrete UO_2 nanoparticles[38] (~2 nm) that are similar in dimensions to the clusters described herein.

Here we introduce a family of **U^{IV}**-oxo-sulfate cluster superlattices. Polyoxoanion clusters assemble with lanthanide (**Ln^{III}**) and transition metal (**TM^{II}**) countercations, where the size and geometry of the polyanion (containing 6, 70 or 84 **U^{IV}**-centers, respectively **U₆**, **U₇₀**, and **U₈₄**) can be rationalized by acidity of the reaction media, and the covalency of the Ln or TM countercation (**figure 1**). **U₈₄**, is a 'cluster-of-clusters' superatom, highlighted in three different superlattices with three generations of self-replicating structures, linked by **Ln^{III}**, **U^{IV}**-monomers and **U₆**. **U₇₀** is a wheel-structure, unlike any prior-reported **U^{IV}**-cluster, that is charge-balanced and assembled with **TM^{II}** (Mn, Zn) in low-acidity media. In three different lattices, these also display complex supramolecular assembly, including sandwiching **U₆**-units. Different bonding behavior of Zn^{2+} and Mn^{2+} to **U₇₀** in the solid-state are preserved in solution, further underlining the importance of these counterions on assembly processes. **U₇₀** and **U₈₄** are the largest tetravalent actinide (or Zr/Hf^{IV}) molecular clusters observed to date, strategically isolated with nonconventional, high-valence countercations.[39]
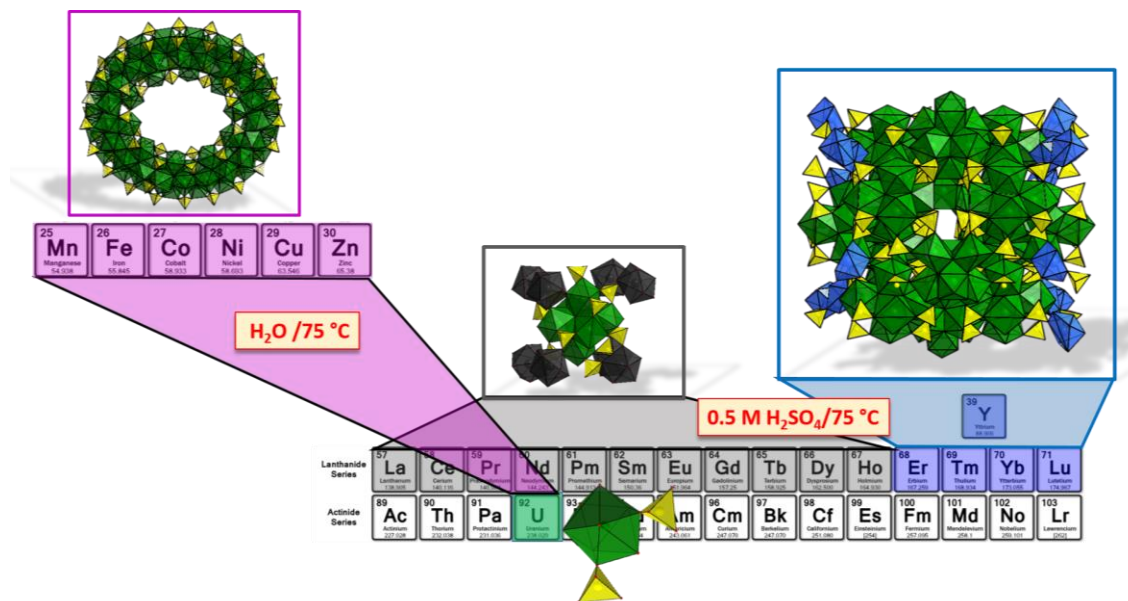
Figure 1. Summary of U^{IV}-sulfate TM/Ln phases. Schematic summarizing the reaction of $U(SO_4)_2$ with (1) divalent transition metals charge-balancing **U_{70}** (top left), (2) large **Ln^{III}** building **U_6**-frameworks (middle), and (3) small **Ln^{III}** charge-balancing **U_{84}** (right). Green and yellow polyhedra are respectively U^{IV}-oxo and SO_4^{2-}, black polyhedra are large **Ln^{III}**-oxo and blue polyhedra are small **Ln^{III}**-oxo. Details of these structures are in subsequent text and figures.

Results and discussion

All tetravalent metals, including **U^{IV}**, exhibit strong hydrolysis behavior. Upon dissolution in water, the highly-charged cations bind water and deprotonate, leading to formation of oligomers, even in aqueous acid.[40] The fundamental hydrolysis and condensation reactions describing this process are: $2OH^- + 2[H_2O-U]^{4+} \rightarrow 2[HO-U]^{3+} + 2H_2O \rightarrow [U-(OH)-U]^{7+} + H_2O$. We dissolved rare earth oxides in the acidic solutions to drive this reaction by the generation of hydroxide, i.e. $La_2O_3 + 3H_2O \rightarrow 2La^{3+} + 6OH^-$. *In-situ* production of hydroxide in this manner is more controlled than adding a strong base, which promotes UO_2-formation, the end-product of hydrolysis-condensation reactions. Additionally, the strongly coordinating sulfate ions in these reactions compete with the hydrolysis reactions, allowing assembly of cluster-based framework materials.

U^{IV}-lanthanide assemblies

Combining larger lanthanides, such as **La^{III}**, leads to the assembly of frameworks consisting of **U_6** that are bridged by the heterometal center. We have crystallized different arrangements of these from Ln = La – Ho. We describe the prototype **La-U_6** here as an example; others will be described in subsequent publications. **La-U_6**, formulated $La_4U_6(OH)_4(O)_4(SO_4)_{12}(H_2O)_{20}$, crystallizes in the monoclinic space group $P2_1/a$ (**Table SI-1**). The **U^{IV}** hexamer is the typical core $[U_6(OH)_4(O)_4)]^{12+}$, exhibiting oxo-hydroxo disorder (fig. SI-1). The first **U_6**-sulfate was reported in 1953;[41] and then not again until very recently.[24] The core **U_6**-sulfate anion (**figure 2a**) is a recurring moiety throughout the structures described here. The charge-balancing **La^{III}** bridge two hexamers via sulfate groups. Each **U_6**-hexamer can be described as a distorted cube, with its six polyhedra occupying the six cube faces, and eight La located on

the cube corners **(figure 2b)**. A framework arises from the 'corner-to-corner' linkages of bridging La-monomers. Due to the 3D-checkerboard linkage, **La-U$_6$** exhibits large voids that contain disordered lattice waters **(figure 2c, Table SI-9)**.
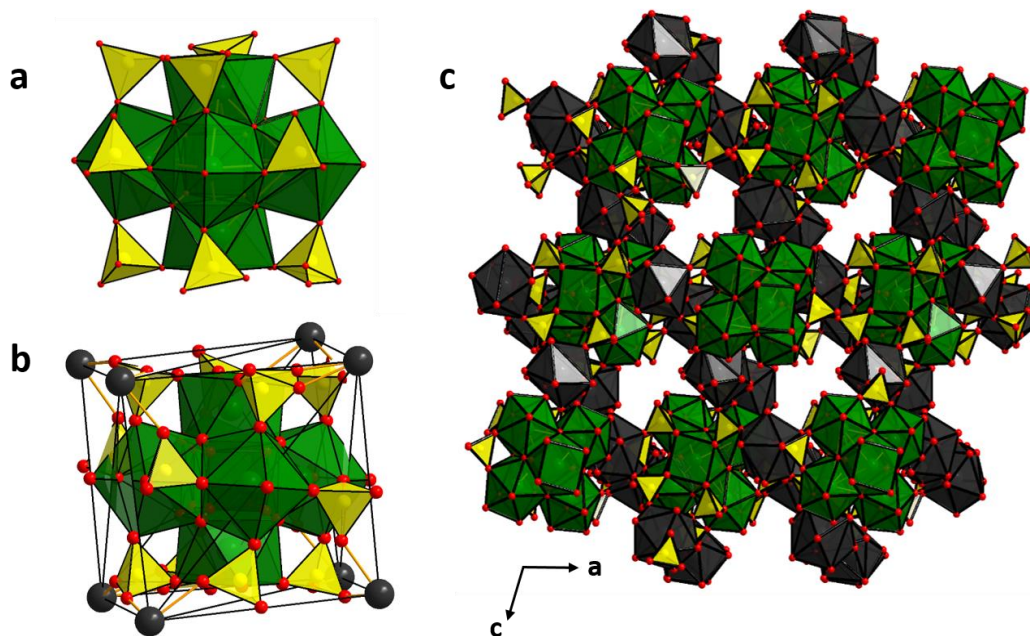
Figure 2. Ln-U$_6$ frameworks. **a)** polyhedral representation of $[U_6(OH)_4(O)_4(SO_4)_{12}]^{12-}$: U^{IV} polyhedra are green, sulfate polyhedra are yellow, O is red spheres. **b)** Highlighting the linkage between La^{III} (black spheres) and **U$_6$**. **c)** Polyhedral representation of **La-U$_6$** framework, showing void channels along the *b*-axis.

With the smaller **Ln^{III}** (Er-Lu & Y) as countercations, a 2nd-generation assembly of **U$_6$** is observed. Fourteen sulfate-bridged **U$_6$**- clusters assemble into a hollow sphere; a **U$_6$** occupying the six faces and the eight corners of a cube **(figure 3a-3b)**, totaling 84 U^{IV}·centers, comprising a **U$_{84}$** superatom. The **U$_6$** of the corner positions, (blue, **U$_{6c}$**) have 12 bridging sulfates, while the face **U$_6$** (green, **U$_{6f}$**) possess 16 sulfates. Each **U$_{6f}$** is linked to four **U$_{6c}$** along the diagonals of the **U$_{84}$**-cube face. Likewise, each **U$_{6c}$** is linked to three **U$_{6f}$**. Each **U$_{6f}$,-U$_{6c}$** linkage is through three bridging sulfates, reinforcing the rigid **U$_{84}$**. We can rationalize this structure switch from lanthanide-linked **U$_6$** frameworks to **U$_{84}$** assemblies that occlude the **Ln^{III}** counterions with a modern description of Ln-bonding that includes covalent bonding contribution from the 5*d* orbitals.[42] Contraction of these orbitals across the series decreases the ability of Ln to participate in covalent network assembly. While La^{III} disrupts linkage between **U$_6$**-units, **Lu^{III}** behaves more as a classic counterion in the superlattice, *vide infra*. Three structures displaying differentiating 3rd-generation assembly of **U$_{84}$** superatoms are described below.

Y-U$_{84}$, formulated $Y_{16}[U_6(OH)_4(O)_4]_{14}(SO_4)_{108}(H_2O)_{126.5}$, crystallizes in the tetragonal *P*4/*m* space group (volume = 39,627 Å^3, **Table SI-2**). Each **U$_{84}$** is surrounded by twelve **U$_{84}$** units, resembling cubic closest packing of equal-sized spheres, defining the 3rd-generation of supramolecular assembly. **U$_{84}$** are bridged by **Y^{III}** via the eight **U$_{6c}$**-corners **(figure 3c)** and four of

the U_{6f}-faces. Y^{III}-monomers (7-8 coordinate) decorate and bridge the U_{84} clusters through sulfate bridges.

$\quad$ **LuU-U$_{84}$**, formulated $U_4Lu_{12}(U_6(OH)_4(O)_4)_{14}(SO_4)_{110}(H_2O)_{80}$ crystallizes in the trigonal R-$3c$ space group (volume = 137,813 Å^3, **Table SI-4**). **LuU-U$_{84}$** can be described as a body centered cubic arrangement of U_{84} (**figure 3d**), linked by U^{IV} monomers that are bridged by corner-sharing sulfates. Partially occupied Lu^{III} also decorates and bridges U_{84} via the sulfates, but the main connectivity is defined by U^{IV}-monomers. Notable is the multiscale replication of patterns: this linking of U_{84} joined by monomers at the eight corner-U_{6c} is similar to the first structure described (**La-U$_6$**), where U_6 are linked by corners via La^{III}-monomers.

$\quad$ **ErU$_6$-(U$_{84}$)$_2$**, formulated $U_6(OH)_4(O)_4(H_2O)_{12}[Er_{16}(U_6(OH)_4(O)_4)_{14}(SO_4)_{111}(H_2O)_{130}]_2$ (**Table SI-3**), crystallizes in the cubic space group Pn-3 (volume = 84,891 Å^3). In **ErU$_6$-(U$_{84}$)$_2$**, rotationally-disordered U_6 (U_{6tet} for this discussion, disorder detailed in the SI) occupies half the tetrahedral voids of closest packed U_{84}, and links to the U_{6c} via sulfate bridges. There are two interpenetrating tetrahedral **ErU$_6$-(U$_{84}$)$_2$** networks, shown in green and blue in **figure 3e**. The U_{84}-units are also connected by Er^{III}-monomer-sulfate-U_{6f} linkages (**figure 3e, inset**).
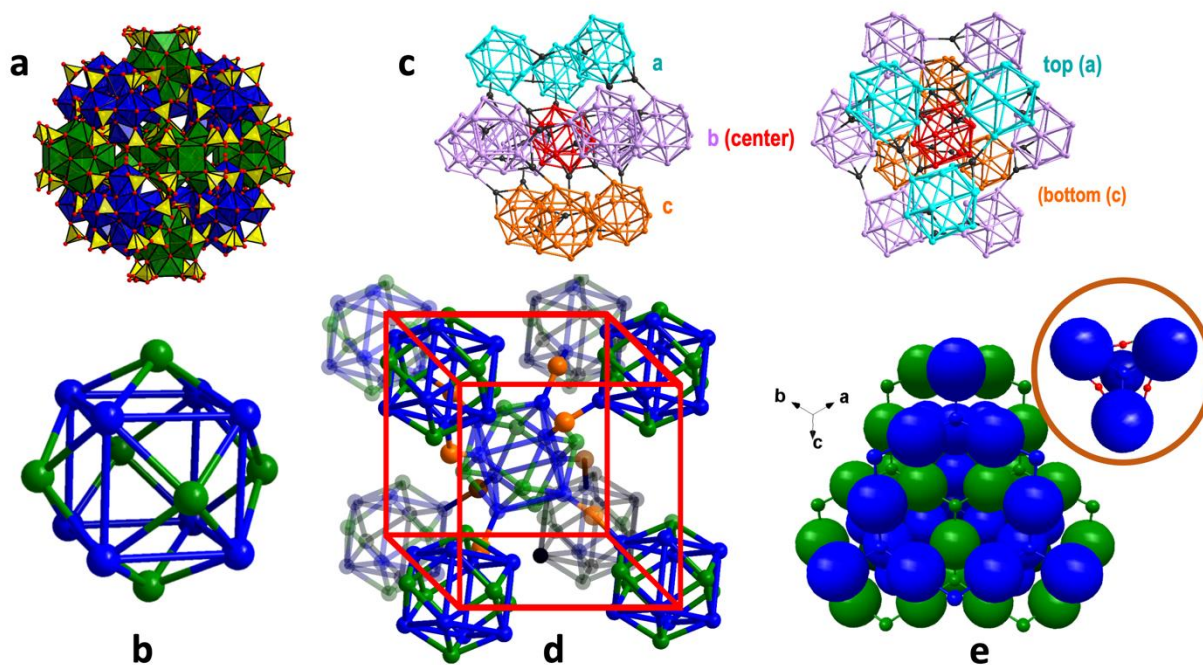

Figure 3. **U$_{84}$ and its superlattices. a)**. Polyhedral representation of **U$_{84}$**. **U$_{6c}$** (corner) are blue, **U$_{6f}$** (face) are green, sulfate is yellow. **b)** Simplified representation of **U$_{84}$**, replacing the **U$_6$** units with green (**U$_{6f}$**) and blue (**U$_{6c}$**) spheres. **c)** View of **Y-U$_{84}$**, highlighting the cubic closest packing of the **U$_{84}$** superatoms, linked by Y-monomers (black spheres). **d)** View of **LuU-U$_{84}$**, highlighting the body-centered cubic arrangement of **U$_{84}$**, bridged by **U^{IV}**-monomers (orange). **e)** Simplified representation of **ErU$_6$-(U$_{84}$)$_2$**, highlighting the two diamondoid interpenetrating networks (respectively green and blue). Large spheres are **U$_{84}$**, linked by **U$_6$** (small spheres). Each tetrahedral network is also bridged by partially-occupied **Er^{III}** (inset, red spheres linking blue network).

U^{IV}-transition metal assemblies

The addition of first row divalent transition metals (TM^{II}, in the form of acetate salts) to the aqueous uranium sulfate salt leads to a different cluster assembly. While 0.5 molar sulfuric acid was optimal to keep the Ln^{III}-U^{IV} reactants dissolved, the first row TM^{II} can dissolve in water only. The lack of coordinating sulfate and lower acidity is conducive to more extensive hydrolysis. However, instead of yielding the end-produced UO_2, TM^{II} stabilizes and charge-balances a U_{70} ring with the core formula $[U_{70}(OH)_{36}(O)_{64}(SO_4)_{60}]^{4-}$ (**figure 1** and **4**). Mn^{II} and Zn^{II} analogues are introduced here, and others will be described in subsequent publications.

The U_{70}-ring features 70 U^{IV} centers fused by oxo/hydroxo ligands. It can be viewed as ten alternating U_6 and U^{IV} monomers (**figure 4a**). The U_6-subunit has the typical core formula of $[U_6(OH)_4(O)_4)]^{12+}$. However, instead of twelve bridging-sulfates, it possesses only eight; four bridging the outer ring and four bridging the inner ring. The outer sulfates link to the U^{IV}-monomer, while the inner sulfates bridge to neighboring hexamers, creating curvature. The entirety of the ring structure exhibits oxo/hydroxo disorder, determined by bond valence sum calculations (**Table SI-11**). All the uranium centers are 8-coordinate with the exception of the innermost uranium of the U_6-units. These are 9-coordinate, due to an additional bound water. Additional terminally-bound sulfates link the rings in an offset 'face-to-face' manner in the different assemblages (**fig. 4d**).
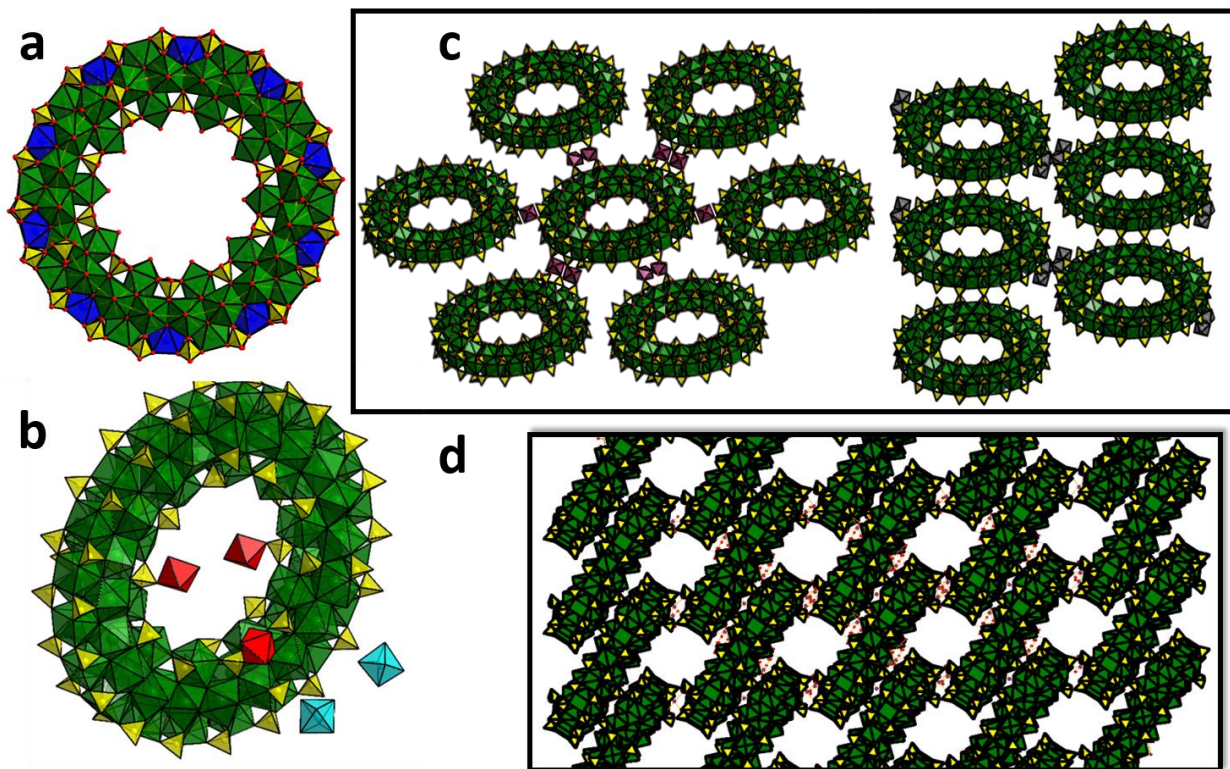
Figure 4. **TM^{II}-U$_{70}$. a)** Polyhedral representation of **U$_{70}$** highlighting the monomer and hexamer units. **U^{IV}** monomer in blue and **U$_6$** unit in green, sulfur in yellow, oxygen in red. **b)** Representation of **Zn-U$_{70}$**, emphasizing the coordination environments of Zn. The red octahedra are Zn linked to **U$_{70}$** via corner-sharing with sulfate. These sit just above the central cavity. The turquoise octahedra are Zn(H$_2$O)$_6$ that are located between **U$_{70}$**-rings, unassociated. **c) Mn-U$_{70}$** and **Zn-U$_{70}$** highlighting the difference in cluster linking via Mn-octahedra (purple) and Zn-polyhedra (gray). **d)** View of **Mn-U$_{70}$** lattice (approximately perpendicular to the viewing direction in **c**.

Mn-U$_{70}$, formulated Mn$_6$U$_{70}$(OH)$_{36}$(O)$_{64}$(SO$_4$)$_{64}$(H$_2$O)$_{44}$, crystallizes in the triclinic *P*-1 space group (volume = 16,367 Å^3, **Table SI-5**). The **U$_{70}$**-rings are stacked offset and face-to-face, approximately along the *a*-direction. They are linked together by both bridging sulfates and **Mn^{II}**-octahedra. The **Mn^{II}**-octahedra also join the stacks together nearly perpendicular to the stacking direction (**figure 4d**), leading to a fully connected framework (**figure 4c**) with large pores (**Table SI-9**).
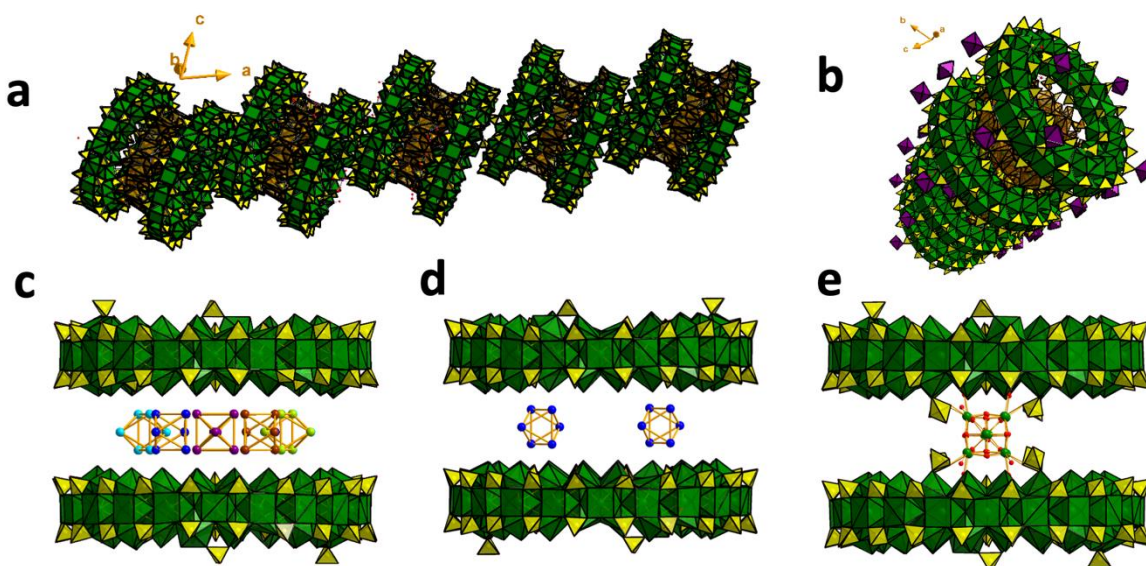
Figure 5 U$_{70}$-U$_6$-U$_{70}$ sandwich. a) View of the U$_{70}$-U$_6$-U$_{70}$ sandwich stacking in **Mn-(U$_6$U$_{70}$)$_2$**. Bright green polyhedra are **U^{IV}** – oxo of **U$_{70}$**, brown polyhedra are the disordered hexamers, yellow polyhedra are sulfate. **b)** Approximately perpendicular view of the **U$_{70}$-U$_6$-U$_{70}$** sandwich stacks, showing linkage of the Mn-octahedra (purple), corner-sharing with sulfate. **c)** View of the five settings of the **U$_6$**-cluster inside the sandwich. Only the uranium, shown in turquoise, blue, purple, brick, and chartreuse (left to right). **d)** Illustration of the 1/5th occupancy of **U$_6$**, as pairs on opposite sides of the wheel. **e)** Highlighting connectivity of **U$_6$** via four sulfate bridges to the **U$_{70}$**-rings.

Mn-U$_{70}$ was obtained via the addition of TBACl (tetrabutylammonium chloride) to the reaction solution, which can mediate the assembly of the **U$_{70}$**-rings, by changing the ionic strength of the system. Without TBA$^+$, we obtain a **U$_{70}$-(U$_6$)$_2$-U$_{70}$** sandwich, **Mn-(U$_6$U$_{70}$)$_2$,** formulated Mn$_4$(H$_2$O)$_{16}$[(U$_6$(OH)$_4$(O)$_4$)(H$_2$O)$_9$)(U$_{70}$(OH)$_{34}$(O)$_{66}$(SO$_4$)$_{65}$(H$_2$O)$_{61}$]$_2$. **Mn-(U$_6$U$_{70}$)$_2$** crystallizes in the triclinic *P*-1 space group (volume = 37,244 Å^3, **Table SI-6**) The **U$_{70}$-(U$_6$)$_2$-U$_{70}$** sandwich contains two **U$_6$**-clusters on opposite sides and between two **U$_{70}$**-rings. Four sulfates of **U$_6$** bridge to the ring on the outside, while the inner association is via hydrogen-bonding between **U$_6$** and **U$_{70}$** (**figure 5c**). The **U$_6$** pairs are disordered over five positions, consistent with the 10-fold symmetry

of the U_{70} ring (**figure 5c**). Details describing this disorder are included in the SI. Chains of the **[U$_{70}$-(U$_6$)$_2$-U$_{70}$]$_n$** run approximately along the *a*-axis (**figure 5a** and **b**), with similar offset of stacking found in **Mn-U$_{70}$**. In addition, the charge-balancing **Mn^{II}**-monomers link the chains of rings in the opposite direction, approximately in the *bc*-plane, via coordination to sulfates of neighboring **U$_{70}$**.

Zn-U$_{70}$ was also obtained with the TBACl 'mineralizer'. It is fully formulated $(Zn(H_2O)_6)_{3.5}Zn_{2.5}U_{70}(OH)_{36}(O)_{64}(SO_4)_{64}(H_2O)_{54.5}$ and crystallizes in the triclinic *P*-1 space group (volume =14,801 Å^3, **Table SI-7**). **Zn-U$_{70}$** presents a similar arrangement in the lattice as **Mn-U$_{70}$** (**figure 4c**). However, an important distinction is the lack of any linking of **U$_{70}$** between or within the stacks via Zn^{2+}. Of the four Zn-sites, two are only fully bonded to water, and the other two bound inside the **U$_{70}$**-ring (**figure 4b**). The $3d^{10}$ of **Zn^{II}** configuration minimizes covalent linkage of the sulfate ligands, as recent in X-ray absorption studies.[43]

Small Angle X-ray Scattering. The extensive **U$_{70}$-Mn^{II}-U$_{70}$** and minimal **U$_{70}$-Zn^{II}-U$_{70}$** connectivity observed in the solid-state compounds was also evidenced upon dissolution. Despite the entirely inorganic nature of the **U$_{70}$**-ring, its aqueous synthesis, and its interconnectivity in various frameworks; it can be dissolved intact in organic media (1:3 THF: butylamine), perhaps because of the extremely low charge density of the cluster (-4 per 70 metal-centers). The small-angle scattering intensity for dissolved **Zn-U$_{70}$** and **Mn-U$_{70}$** is strong due to their large size and the presence of strongly scattering uranium (**figure 6b**). The average-size species for dissolved **Mn-U$_{70}$** is considerably larger than that for **Zn-U$_{70}$**, indicated by the Guinier region shift to lower-q for the former. The Guinier region is the steep negative-slope at low-q (q<.0.15 Å^{-1} for **Mn-U$_{70}$**; q<.0.20 Å^{-1} for **Zn-U$_{70}$**). The **Mn-U$_{70}$** curve is ideally fit with a core-shell cylindrical model (**Table SI-12, fig. SI-9**) that matches well with simulated scattering data for a hypothetical stack of eight **U$_{70}$**-rings. We can confidently say this is the main aggregate present in this solution, and that Mn^{II} links the clusters, in addition to the sulfate. Comparing the **Zn-U$_{70}$** scattering to the simulated **U$_{70}$**-monomer scattering shows a good match between ~q=0.1-0.8 Å^{-1}. Moreover, the two plateaus between ~q=0.2-0.2 Å^{-1} are observed in both the simulated and experimental scattering—strong evidence that the **Zn-U$_{70}$** solution is dominated by isolated clusters. However, the upward slope at q > 0.1 Å^{-1} indicates formation of aggregates. Analysis of the size distribution suggests the majority of the dissolved aggregates are around 35 Å (**U$_{70}$**-monomers) in diameter, with a larger population of ~80 Å (ratio of **U$_{70}$**:aggregates ~9:1, **fig. 6c**). Based on inspecting and simulating SAXS data for various **U$_{70}$**-aggregates observed in the crystal structures, we propose the modest amount linking promoted by Zn is via staggered stacking rather than perfectly eclipsed, as observed for dissolved **Mn-U$_{70}$**. The oscillations and other features at high-q (i.e. the peaks around 2 Å^{-1}) that give information on shape and atom-atom distances are also present in both the experimental and simulated datasets. It is interesting that the eclipsed stacking that is so prevalent in the **Mn-U$_{70}$** solution has not been observed in solid-state structures presented here, nor in other structures we have obtained that will be reported shortly. Perhaps the butylamine stabilizes the cylindrical stacks via inverse micelle formation. This suggests other supramolecular assemblies may be accessible

via dissolution of U_{70} in organic media containing various TM-linkers and surfactants. This is a similar strategy used prior to create superlattices of nanoparticles.[44, 45]
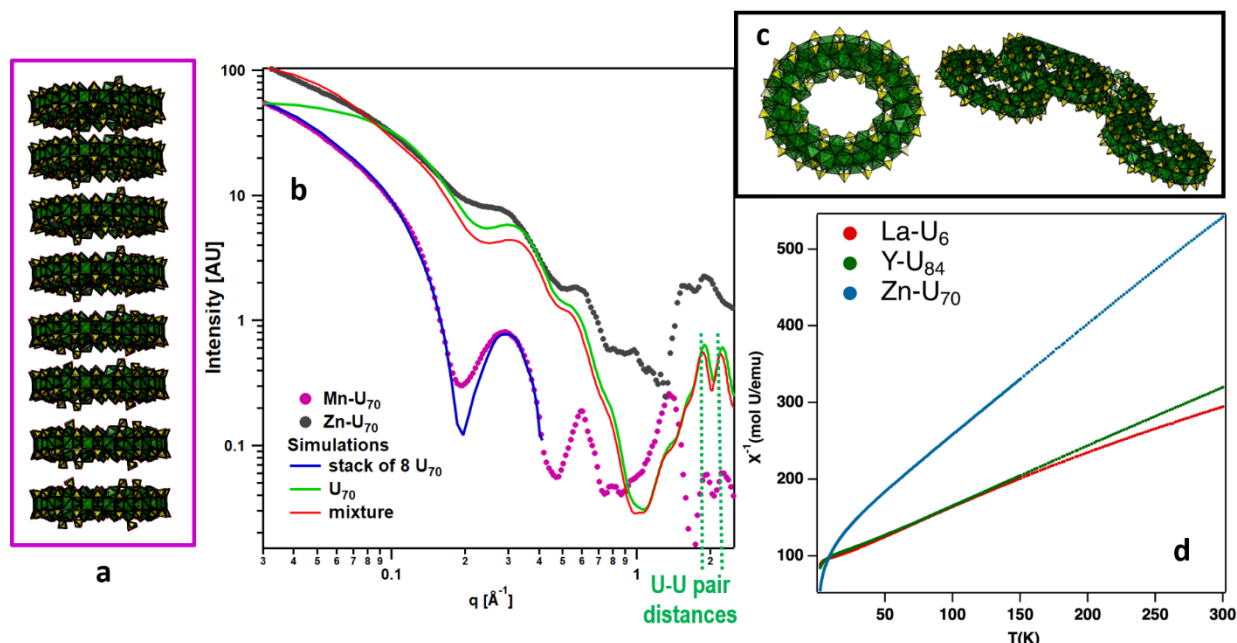
Figure 6. X-ray scattering of dissolved U_{70} and Magnetic Susceptibility a) Hypothetical stack of eight U_{70}, its simulated scattering data matches that of **Mn-U_{70}** (simulated scattering shown in blue in b). . **b)** Experimental scattering data for **Mn-U_{70}** (pink) and **Zn-U_{70}** (black) in 1:3 THF:butylamine solvent mixture. **c)** Isolated U_{70} (simulated scattering data in green), plus aggregate of four U_{70}; $[U_{70}]_4$. Simulated scattering data for 90% U_{70} and 10% $[U_{70}]_4$ is shown in red. This approximate mixture is proposed for dissolved **Zn-U_{70}**, as determined by size distribution analysis of experimental scattering data (see **fig SI-10**. **d)** Magnetic susceptibilities of **La-U_6, Y-U_{84}, Zn-U_{70}** measured under zfc conditions and an applied field of 1000 Oe.

Magnetic measurements. While magnetic ordering and frustration has been discovered in polynuclear TM, Ln and TM-Ln single-molecule magnets,[46] similar studies of An-TM/Ln have been less explored, partly due to a paucity of synthesized species. In fact, only one measurement of U^{IV}-oxo clusters (U_6)[47] and very recently U_{38},[48] has been executed. Similar to U^{IV}-oxides, U_6 and U_{38} exhibit transition of the $5f^2$ electrons from unpaired to paired with cooling. Typically, high coordination U^{IV}-compounds (CN = 8) exhibit Curie-Weiss behavior[49] whereas lower coordination numbers (CN = 6) lead to non-Curie-like behavior due to strong crystalline electric field effects.[50] Recently, a Mn-U^{IV} fluoride was described with magnetic coupling between the $3d$ and $5f$ electrons,[51] piquing interest in magnetic properties of U^{IV}-TM/Ln oxo-clusters and oxides.

Figure 6d shows the magnetic susceptibility of **La-U_6, Y-U_{84}, Zn-U_{70},** and **Mn-U_{70}** and the magnetic data is summarized in **Table 1**. In the first three compounds, U^{IV} is the only magnetic ion, allowing for direct observation of the U^{IV} magnetic behavior. All three compounds exhibit Curie-Weiss behavior at high temperatures, without pairing of the $5f^2$-electrons down to 2 K. Fitting the 50-300 K data to the Curie-Weiss law yields effective moments of 3.58(3) μ_B/U (**La-U_6**), 3.19(3) μ_B/U (**Y-U_{84}**), and 2.36(3) (**Zn-U_{70}**). Because of the non-Curie like behavior of many U^{IV}-compounds, the uranium moment is often estimated as $2.827(\chi T)^{1/2}$ at 300 K, yielding moments reported in **Table 1**. The observed moment for **La-U_6** extracted from the Curie-Weiss fit

is in excellent agreement with the calculated moment of 3.58 μB/U for U^{IV}, and the others are within the reported ranges.[52] Variations correlate with U^{IV}-coordination. The largest is observed for **La-U₆**, in which the majority of the U^{IV}-sites are 9-coordinate (four of six), and the lowest is observed for **Zn-U₇₀**, in which the U sites are predominately 8-coordinate (56 of 70). **Y-U₈₄**, with an intermediate moment, contains almost half 8-coordinate U sites (48 of 84). All three compounds have large, negative paramagnetic Curie-Weiss temperatures, likely due to crystalline-electric field effects. The magnetic susceptibility of **Mn-U₇₀** likewise exhibits Curie-Weiss behavior at high temperatures, however no magnetic ordering is observed down to 2 K.

Table 1 Magnetic properties of reported phases. All data fit to the Curie-Weiss law from 50-300K.

	θ (K)	μ_{eff} (μB/F.U.)	μ_{calc} (μB/F.U.)	μ_{eff} (μB/U)	μ_{calc} (μB/U)
La-U₆	-140(3)	-	-	3.58(3)	3.58
Y-U₈₄	-112(3)	-	-	3.21(3)	3.58
Zn-U₇₀	-79(2)	-	-	2.36(3)	3.58
Mn-U₇₀	-28.2(6)	27.93(9)	33.28	2.85(3)[a]	3.58

[a]Calculated assuming an observed moment of 5.92 μB/Mn

The **TM^{II}** and **Ln^{III}** U^{IV}-sulfate compounds described here are representative of a larger family that will be subsequently reported. As represented here, this family features **U₈₄**, a 'superatom' that organizes into superlattices with both heteroatom monomers and the **U₆** unit of **U₈₄.** Superlattices assembled with small **Ln^{III}** include tetrahedral (interpenetrating), body-centered cubic and cubic-closest packed networks of **U₈₄**. The body-centered **U₈₄** network-type mirrors **U₆** networks with large **Ln^{III}**. **U₈₄**, comprised of 14 linked **U₆**, mirrors the arrangement of the U^{IV}-monomers and sulfate bridges in **U₆**; and, thus, superlattices of **U₈₄** can also be described as fractals with three generations. Because the closest U^{IV}-Ln or U^{IV}-TM connectivity is via a sulfate bridge in the reported compounds, there is no magnetic exchange or ordering. One future goal is to minimize or replace the sulfate in our syntheses, and also promote isolation of U^{V}-containing analogues to access targeted magnetic synthons. The **U₇₀** ring is a **M^{IV}** (M=Zr/Hf/An) cluster genre that has never been observed, and also displays unique non-aqueous solubility and differing supramolecular assembly via **TM^{II}**-counterion linking. We will also access new superlattices of **U₈₄** and **U₇₀** from organic media, driving assembly from organic capping groups, as well as polyvalent counterion-linking.

Methods After discovering the initial crystalline forms, the syntheses with Ln were adjusted and optimized for yield and purity. In the optimized experiments, we combined mixtures of the oxides and chloride salts of the various lanthanides (see methods sections). Optimized syntheses are summarized here, details are provided in the SI, along with procedures for single-crystal X-ray diffraction, magnetic measurements, and SAXS, IR vibration spectroscopy, and TGA.

$U(SO_4)_2$, the reactant for all subsequent syntheses, is prepared from 5.0 g of uranyl(VI) acetate in 75 mL of anhydrous ethanol plus 25 mL of concentrated sulfuric acid. This solution is placed under UV light (390-400 nm, 15 W) for 24-48 hours to obtain a green/purple U^{IV} sulfate powder. The solid is collected by vacuum filtration and washing with four 50 mL aliquots of ethanol. (yield = 95.5%)

The **Ln-U^{IV}** (**U_6** and **U_{84}**) compounds were all synthesized by similar methods, described generally here with details in the SI. $U(SO_4)_2$ (100 mg, 0.23 mmol) is dissolved in 500 µL of 0.5 M H_2SO_4 in a 2 mL vial. The Ln is introduced as optimized mixtures of Ln_2O_3 plus $LnCl_3$. The vial is then placed in a sand bath and heated in an oven at 75 ˚C for 24 h. Crystalized products are then filtered out and washed with water followed by 0.5 M HCl to remove any soluble byproduct or starting material.

The **TM-U^{IV}** compounds (**U_{70}**) were synthesized as follows (details in SI). 100mg of $U(SO_4)_2$ (0.23 mmol) is dissolved in 500 µL of H_2O in a 2 mL vial. TM^{II} (Zn, Mn) acetate was added and the vial is then placed in a sand bath and heated in an oven at 75 ˚C for 24 h.

Author Contributions

IC and MN conceived the experiments, analyzed the data and wrote the paper. IC carried out all experiments except magnetic measurements. GM and HZL provided the magnetic measurements, data interpretation and written contribution to the manuscript.

Competing interests

The authors declare no competing interests

Additional information

Supplementary information is available for this paper at ….

References

1. Wang L, Liu R, Gu JL, Song B, Wang H, Jiang X, *et al.* Self-Assembly of Supramolecular Fractals from Generation 1 to 5. *J Am Chem Soc* 2018, **140**(43)**:** 14087-14096.

2. Yang HB, Northrop BH, Zheng YR, Ghosh K, Stang PJ. Facile Self-Assembly of Neutral Dendritic Metallocycles via Oxygen-to-Platinum Coordination. *J Org Chem* 2009, **74**(18)**:** 7067-7074.

3.   Caminade AM, Yan DY, Smith DK. Dendrimers and hyperbranched polymers. *Chem Soc Rev* 2015, **44**(12)**:** 3870-3873.

4.   Newkome GR, Yao ZQ, Baker GR, Gupta VK. Micelles .1. Cascade Molecules - a New Approach to Micelles - a [27]-Arborol. *J Org Chem* 1985, **50**(11)**:** 2003-2004.

5.   Tomalia DA, Naylor AM, Goddard WA. Starburst Dendrimers - Molecular-Level Control of Size, Shape, Surface-Chemistry, Topology, and Flexibility from Atoms to Macroscopic Matter. *Angew Chem Int Edit* 1990, **29**(2)**:** 138-175.

6.   Golub E, Subramanian RH, Esselborn J, Alberstein RG, Bailey JB, Chiong JA*, et al.* Constructing protein polyhedra via orthogonal chemical interactions. *Nature* 2020.

7.   Peng Q, Dong YJ, Deng ZX, Li YD. Selective synthesis and characterization of CdSe nanorods and fractal nanocrystals. *Inorg Chem* 2002, **41**(20)**:** 5249-5254.

8.   Shahzad A, Bhang SH, Jung E, Kim WS, Yu T. Hierarchically structured 2D silver sheets with fractal network. *J Materiomics* 2018, **4**(2)**:** 121-128.

9.   Rosseinsky MJ. Fullerene Intercalation Chemistry. *J Mater Chem* 1995, **5**(10)**:** 1497-1513.

10.   Claridge SA, Castleman AW, Khanna SN, Murray CB, Sen A, Weiss PS. Cluster-Assembled Materials. *Acs Nano* 2009, **3**(2)**:** 244-255.

11.   Liu C, Sun ZM. Recent advances in structural chemistry of Group 14 Zintl ions. *Coordin Chem Rev* 2019, **382:** 32-56.

12.   Mandal S, Reber AC, Qian M, Liu R, Saavedra HM, Sen S*, et al.* Synthesis, structure and band gap energy of covalently linked cluster-assembled materials. *Dalton T* 2012, **41**(40)**:** 12365-12377.

13.   Qian MC, Reber AC, Ugrinov A, Chaki NK, Mandal S, Saavedra HM*, et al.* Cluster-Assembled Materials: Toward Nanomaterials with Precise Control over Properties. *Acs Nano* 2010, **4**(1)**:** 235-240.

14.   Cavka JH, Jakobsen S, Olsbye U, Guillou N, Lamberti C, Bordiga S*, et al.* A new zirconium inorganic building brick forming metal organic frameworks with exceptional stability. *J Am Chem Soc* 2008, **130**(42)**:** 13850-13851.

15. Shepelev YF, Smolin YI, Ershov AS, Rademaher O, Sheller G. Determination of the Crystal-Structure of Sodiumtetramethylammonium Silicate Na.7[N(Ch3)4][Si8o20].54h2o at -120-Degrees-C. *Kristallografiya+* 1987, **32**(6)**:** 1399-1403.

16. Smolin II, Shepelev IF, Ershov AS, Hoebbel D. Isolated Aluminosilicate Radical [Si4al4o12(Oh)8] in the Tetramethylammonium Aluminosilicate Crystal. *Dokl Akad Nauk Sssr+* 1987, **297**(6)**:** 1377-1380.

17. Fedeyko JM, Vlachos DG, Lobo RF. Formation and structure of self-assembled silica nanoparticles in basic solutions of organic and inorganic cations. *Langmuir* 2005, **21**(11)**:** 5197-5206.

18. Mollick S, Fajal S, Mukherjee S, Ghosh SK. Stabilizing Metal-Organic Polyhedra (MOP): Issues and Strategies. *Chem-Asian J* 2019, **14**(18)**:** 3096-3108.

19. Vardhan H, Yusubov M, Verpoort F. Self-assembled metal-organic polyhedra: An overview of various applications. *Coordin Chem Rev* 2016, **306:** 171-194.

20. Kalaji A, Soderholm L. Aqueous Hafnium Sulfate Chemistry: Structures of Crystalline Precipitates. *Inorg Chem* 2014, **53**(20)**:** 11252-11260.

21. Knope KE, Vasiliu M, Dixon DA, Soderholm L. Thorium(IV)-Selenate Clusters Containing an Octanuclear Th(IV) Hydroxide/Oxide Core. *Inorg Chem* 2012, **51**(7)**:** 4239-4249.

22. Knope KE, Wilson RE, Vasiliu M, Dixon DA, Soderholm L. Thorium(IV) Molecular Clusters with a Hexanuclear Th Core. *Inorg Chem* 2011, **50**(19)**:** 9696-9704.

23. Falaise C, Kozma K, Nyman M. Thorium Oxo-Clusters as Building Blocks for Open Frameworks. *Chem-Eur J* 2018, **24**(53)**:** 14226-14232.

24. Yue Z, Guo X, Feng ML, Lin YJ, Ju Y, Lin X*, et al.* Unexpected Roles of Alkali-Metal Cations in the Assembly of Low-Valent Uranium Sulfate Molecular Complexes. *Inorg Chem* 2020.

25. Lin J, Jin GB, Soderholm L. Th-3[Th-6(OH)(4)O-4(H2O)(6)](SO4)(12)(H2O)(13): A Self-Assembled Microporous Open-Framework Thorium Sulfate. *Inorg Chem* 2016, **55**(20)**:** 10098-10101.

26. Falaise C, Charles JS, Volkringer C, Loiseau T. Thorium Terephthalates Coordination Polymers Synthesized in Solvothermal DMF/H2O System. *Inorg Chem* 2015, **54**(5)**:** 2235-2242.

27. Loiseau T, Mihalcea I, Henry N, Volkringer C. The crystal chemistry of uranium carboxylates. *Coordin Chem Rev* 2014, **266:** 69-109.

28. Ejegbavwo OA, Martin CR, Olorunfemi OA, Leith GA, Ly RT, Rice AM, *et al.* Thermodynamics and Electronic Properties of Heterometallic Multinuclear Actinide-Containing Metal-Organic Frameworks with "Structural Memory". *J Am Chem Soc* 2019, **141**(29)**:** 11628-11640.

29. Martin NP, Marz J, Feuchter H, Duval S, Roussel P, Henry N, *et al.* Synthesis and structural characterization of the first neptunium based metal-organic frameworks incorporating {Np6O8} hexanuclear clusters. *Chem Commun* 2018, **54**(51)**:** 6979-6982.

30. Biswas B, Mougel V, Pecaut J, Mazzanti M. Base-Driven Assembly of Large Uranium Oxo/Hydroxo Clusters. *Angew Chem Int Edit* 2011, **50**(25)**:** 5744-5747.

31. Dufaye M, Martin NP, Duval S, Volkringer C, Ikeda-Ohno A, Loiseau T. Time-controlled synthesis of the 3D coordination polymer U(1,2,3-Hbtc)(2) followed by the formation of molecular poly-oxo cluster {U-14} containing hemimellitate uranium(iv). *Rsc Adv* 2019, **9**(40)**:** 22795-22804.

32. Falaise C, Volkringer C, Vigier JF, Beaurain A, Roussel P, Rabu P, *et al.* Isolation of the Large {Actinide}(38) Poly-oxo Cluster with Uranium. *J Am Chem Soc* 2013, **135**(42)**:** 15678-15681.

33. Martin NP, Volkringer C, Henry N, Trivelli X, Stoclet G, Ikeda-Ohno A, *et al.* Formation of a new type of uranium(iv) poly-oxo cluster {U-38} based on a controlled release of water via esterification reaction. *Chem Sci* 2018, **9**(22)**:** 5021-5032.

34. Sigmon GE, Hixon AE. Extension of the Plutonium Oxide Nanocluster Family to Include {Pu-16} and {Pu-22}. *Chem-Eur J* 2019, **25**(10)**:** 2463-2466.

35. Soderholm L, Almond PM, Skanthakumar S, Wilson RE, Burns PC. The structure of the plutonium oxide nanocluster [Pu38O56Cl54(H2O)(8)](14-). *Angew Chem Int Edit* 2008, **47**(2)**:** 298-302.

36. Martin NP, Volkringer C, Roussel P, Marz J, Hennig C, Loiseau T, *et al.* {Np-38} clusters: the missing link in the largest poly-oxo cluster series of tetravalent actinides. *Chem Commun* 2018, **54**(72)**:** 10060-10063.

37. Novikov AP, Kalmykov SN, Utsunomiya S, Ewing RC, Horreard F, Merkulov A, *et al.* Colloid transport of plutonium in the far-field of the Mayak Production Association, Russia. *Science* 2006, **314**(5799)**:** 638-641.

38. Suzuki Y, Kelly SD, Kemner KM, Banfield JF. Radionuclide contamination - Nanometre-size products of uranium bioreduction. *Nature* 2002, **419**(6903)**:** 134-134.

39. Misra A, Kozma K, Streb C, Nyman M. Beyond Charge Balance: Counter-Cations in Polyoxometalate Chemistry. *Angew Chem Int Edit* 2020, **132**(2)**:** 596-612.

40. Knope KE, Soderholm L. Solution and Solid-State Structural Chemistry of Actinide Hydrates and Their Hydrolysis and Condensation Products. *Chem Rev* 2013, **113**(2)**:** 944-994.

41. Lundgren G. The Crystal Structure of $U_6O_4(OH)_4(SO_4)_6$. *Ark Kemi* 1953, **5:** 349– 363.

42. Loble MW, Keith JM, Altman AB, Stieber SCE, Batista ER, Boland KS*, et al.* Covalency in Lanthanides. An X-ray Absorption Spectroscopy and Density Functional Theory Study of $LnCl(6)(x-)$ (x=3, 2). *J Am Chem Soc* 2015, **137**(7)**:** 2506-2523.

43. Frank P, Szilagyi RK, Gramlich V, Hsu HF, Hedman B, Hodgson KO. Spin-Polarization-Induced Preedge Transitions in the Sulfur K-Edge XAS Spectra of Open-Shell Transition-Metal Sulfates: Spectroscopic Validation of sigma-Bond Electron Transfer. *Inorg Chem* 2017, **56**(3)**:** 1080-1093.

44. Shevchenko EV, Talapin DV, Murray CB, O'Brien S. Structural characterization of self-assembled multifunctional binary nanoparticle superlattices. *J Am Chem Soc* 2006, **128**(11)**:** 3620-3637.

45. Chen Z, O'Brien S. Structure direction of II-VI semiconductor quantum dot binary nanoparticle superlattices by tuning radius ratio. *Acs Nano* 2008, **2**(6)**:** 1219-1229.

46. Sessoli R, Powell AK. Strategies towards single molecule magnets based on lanthanide ions. *Coordin Chem Rev* 2009, **253**(19-20)**:** 2328-2341.

47. Vanagas NA, Wacker JN, Rom CL, Glass EN, Colliard I, Qiao YS*, et al.* Solution and Solid State Structural Chemistry of Th(IV) and U(IV) 4-Hydroxybenzoates. *Inorg Chem* 2018, **57**(12)**:** 7259-7269.

48. Knope KE, Vanagas NA, Higgins RF, Wacker JN, Romar D, Asuigui C*, et al.* Mononuclear to Polynuclear U(IV) Structural Units: Effects of Reaction Conditions on U-Furoate Phase Formation. *Chem-Eur J* 2020.

49. Usman M, Morrison G, Klepov VV, Smith MD, zur Loye HC. Flux crystal growth, structure, magnetic and optical properties of a family of alkali uranium(IV) phosphates. *J Solid State Chem* 2019, **270:** 19-26.

50. Morrison G, Ramanantoanina H, Urland W, Smith MD, zur Loyet HC. Flux Synthesis, Structure, Properties, and Theoretical Magnetic Study of Uranium(IV)-Containing $A_2USi(6)O(15)$ (A = K, Rb) with an Intriguing Green-to-Purple, Crystal-to-Crystal Structural Transition in the K Analogue. *Inorg Chem* 2015, **54**(11)**:** 5504-5511.

51.   Klepov VV, Pace KA, Calder S, Felder JB, zur Loye HC. 3d-Metal Induced Magnetic Ordering on U(IV) Atoms as a Route toward U(IV) Magnetic Materials. *J Am Chem Soc* 2019, **141**(9)**:** 3838-3842.

52.   Kindra DR, Evans WJ. Magnetic Susceptibility of Uranium Complexes. *Chem Rev* 2014, **114**(18)**:** 8865-8882.